ISSN 1063-7834, Physics of the Solid State, 2015, Vol. 57, No. 3, pp. 569–575. © Pleiades Publishing, Ltd., 2015.
Original Russian Text © E.V. Eremin, N.V. Volkov, V.L. Temerov, I.A. Gudim, A.F. Bovina, 2015, published in Fizika Tverdogo Tela, 2015, Vol. 57, No. 3, pp. 556–561.

MAGNETISM

Specific Features of Magnetic Properties of Rare-Earth Ferroborates $Sm_{1-x}La_xFe_3(BO_3)_4$

E. V. Eremin[a, b, *], N. V. Volkov[a, b], V. L. Temerov[a], I. A. Gudim[a], and A. F. Bovina[a]

[a] *Kirensky Institute of Physics, Siberian Branch of the Russian Academy of Sciences, Akademgorodok 50–38, Krasnoyarsk, 660036 Russia*

* *e-mail: eev@iph.krasn.ru*

[b] *Siberian Federal University, Svobodnyi pr. 79, Krasnoyarsk, 660041 Russia*

Received September 11, 2014

Abstract—Single crystals of rare-earth ferroborates $Sm_{1-x}La_xFe_3(BO_3)_4$ ($x = 0$, 0.5, 0.75) have been grown by the flux method. Their magnetic properties have been investigated in the temperature range from 2 to 300 K in magnetic fields up to 9 T. It has been found that the substitution of nonmagnetic ions La^{3+} for magnetic ions Sm^{3+} in $Sm_{1-x}La_xFe_3(BO_3)_4$ ferroborates leads to an increase in the magnetic susceptibility of the compound. The behavior of the magnetic properties of the grown single crystals has been explained qualitatively in the framework of the phenomenological model. The parameters of *d–d* and *d–f* exchange interactions have been estimated.

DOI: 10.1134/S1063783415030051

1. INTRODUCTION

In recent years, rare-earth ferroborates with the huntite structure of the general formula $RFe_3(BO_3)_4$ (R = Y, La–Lu) have attracted increasing attention due to the discovery of multiferroic properties in these compounds [1, 2]. The main structural units of rare-earth ferroborates (space group $R32$) are helical chains formed by edge-sharing FeO_6 octahedra and oriented along the c axis. Bonds between the Fe^{3+} ions along a chain and between chains are such that the exchange interaction within the chain is stronger than the interaction between the chains. Magnetically, rare-earth ferroborates are antiferromagnets with two interacting magnetic subsystems (the subsystem of a rare-earth element and the subsystem of iron). The iron subsystem is ordered at the Néel temperature $T_N = 30$–40 K. The rare-earth subsystem is magnetized by the *f–d* interaction and makes a significant contribution to the magnetic anisotropy and the orientation of magnetic moments. Rare-earth ferroborates can have an easy-axis magnetic structure or an easy-plane magnetic structure, or, as in the case of ferroborates $GdFe_3(BO_3)_4$ and $HoFe_3(BO_3)_4$, they can undergo a spontaneous spin-reorientation transition from the easy-axis state to the easy-plane state with a variation in the temperature [3, 4].

Recent interest expressed in samarium ferroborate $SmFe_3(BO_3)_4$ is caused by the fact that, among all ferroborates with one type of rare-earth ion, this compound exhibits the strongest magnetoelectric effect [5] and giant magnetodielectric effect [6]. All information on spectroscopic, magnetic, resonance, magnetoelectric, and magnetoelastic properties [5–10] indicates that the magnetic moments of iron ions in $SmFe_3(BO_3)_4$ are antiferromagnetically ordered at the temperature $T_N = 32$ K and lie in the basal *ab* plane perpendicular to the c axis of the crystal. Moreover, in the basal plane, there are magnetic moments of the samarium ions magnetized by the exchange field of the iron subsystem. The magnetic moments of iron and samarium ions, which were obtained in [10] from the analysis of the neutron diffraction data on $SmFe_3(BO_3)_4$ powders by assuming the collinearity of all magnetic moments, are equal to 4.2 and 0.24 μ_B at a temperature of 1.7 K, respectively.

For the understanding of the role of Sm^{3+} ions in the formation of the magnetic structure, spontaneous polarization, magnetoelectric polarization, and giant magnetoelectric effect in $SmFe_3(BO_3)_4$, it is necessary to perform further investigation and comparative analysis of ferroborates with the sequential replacement of samarium ions by other rare-earth elements, in particular, by a convenient substituting element, namely, lanthanum. First, lanthanum is a nonmagnetic element and, therefore, will have no effect on the magnetic anisotropy in $Sm_{1-x}La_xFe_3(BO_3)_4$ crystal. Second, among the rare-earth elements, lanthanum has the largest ionic radius, which can affect the mobility of cations in a local anion environment and, consequently, will lead to a change in the magnetoelectric properties.

This paper presents the results of the investigation of the magnetic properties of $Sm_{1-x}La_xFe_3(BO_3)_4$ ($x =$ 0, 0.5, 0.75) single crystals. Further investigations of

Table 1. Composition of the fluxes in the quasi-binary form (100-n) wt % $\{Bi_2Mo_3O_{12} + pB_2O_3 + q[(1 - x)Sm_2O_3 + xLa_2O_3]\} + n$ wt % $Sm_{1-x}La_xFe_3(BO_3)_4$

x	n	p	q
0	20	3	0.5
0.5	22	3	0.5
0.75	21	3	0.6

Designations: x is the degree of substitution of La ions for Sm ions; n is the concentration of crystal-forming oxides (in accordance with the stoichiometry) in wt %; and p and q are the fitted coefficients in terms of the number of moles per mole of $Bi_2Mo_3O_{12}$.

Table 2. Lattice parameters of $Sm_{1-x}La_xFe_3(BO_3)_4$ single crystals at $T = 293$ K

Single crystal	a, Å	c, Å
$SmFe_3(BO_3)_4$ [12]	9.5663	7.5896
$Sm_{0.5}La_{0.5}Fe_3(BO_3)_4$	9.5990	7.6167
$Sm_{0.25}La_{0.75}Fe_3(BO_3)_4$	9.6077	7.6276

the spontaneous polarization, giant magnetodielectric effect, and magnetoelectric polarization will provide additional information about the mechanisms of magnetoelectric coupling in rare-earth ferroborates with the huntite structure.

2. SAMPLE PREPARATION AND EXPERIMENTAL TECHNIQUE

Single crystals of $Sm_{1-x}La_xFe_3(BO_3)_4$ ferroborates were grown from fluxes based on bismuth trimolybdate $Bi_2Mo_3O_{12}$ [11]. The composition of the fluxes in the quasi-binary form, the concentration n of the crystal-forming oxides (in accordance with the stoichiometry of $Sm_{1-x}La_xFe_3(BO_3)_4$), and the coefficients p and q are presented in Table 1.

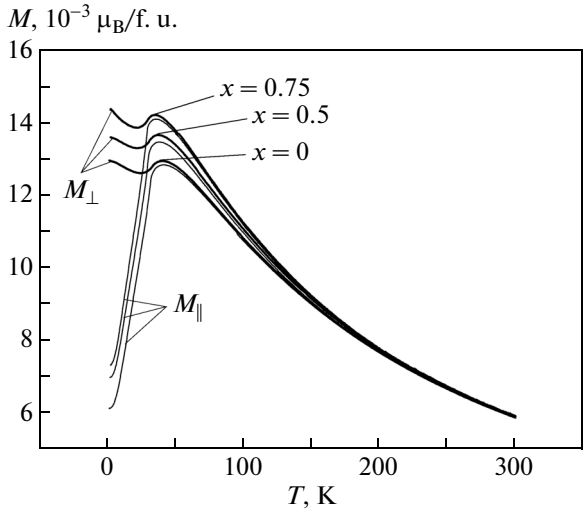

Fig. 1. Temperature dependences of the magnetization of $Sm_{1-x}La_xFe_3(BO_3)_4$ single crystals measured in a magnetic field of 0.1 T for the magnetic field orientations $\mathbf{B} \parallel \mathbf{c}$ and $\mathbf{B} \perp \mathbf{c}$.

Single crystals were grown in two stages. At the first stage, crystals with a size of ~1 mm were grown under spontaneous nucleation conditions. Visually high-quality crystals were then used as a seed. At the second stage, crystals were grown on seeds with a decrease in the temperature so that the growth rate would not exceed 1 mm/day. At the end of the growth, the crystals were cooled to room temperature at a rate of no more than 100°C/h.

The magnetic properties of the grown single crystals were investigated on a Quantum Design PPMS-9 vibrating-sample magnetometer in the temperature range from 2 to 300 K in magnetic fields up to 9 T.

The X-ray diffraction analysis was performed at room temperature on a Bruker D8 ADVANCE X-ray diffractometer (CuK_α radiation) using a powder obtained by grinding $Sm_{1-x}La_xFe_3(BO_3)_4$ single crystals.

3. EXPERIMENTAL RESULTS

It is known [4] that, at high temperatures, all crystals of the $RFe_3(BO_3)_4$ family have a trigonal structure with space group $R32$. In compounds with a large ionic radius (R = La–Sm), this structure remains unchanged down to low temperatures, whereas compounds with a small ionic radius (R = Eu–Er) undergo a structural phase transition $R32 \longrightarrow P3_121$, the temperature of which increases with a decrease in the ionic radius [12].

It can be expected with high probability that the doping with lanthanum ions (which have the ionic radius larger than the ionic radius of Sm^{3+} ions) will lead to an effective increase in the radius of the rare-earth cation as well as to the absence of structural transition in $Sm_{1-x}La_xFe_3(BO_3)_4$. The X-ray diffraction analysis of the $Sm_{0.5}La_{0.5}Fe_3(BO_3)_4$ and $Sm_{0.25}La_{0.75}Fe_3(BO_3)_4$ samples confirmed their phase purity and also the fact that all the observed reflections were indexed by one phase of space group $R32$. The lattice parameters determined in this work are presented in Table 2 in comparison with the lattice parameters taken from [12] for the nominally pure $SmFe_3(BO_3)_4$ single crystal. It can be seen from this table that the lattice parameters increase linearly with an increase in the concentration of lanthanum ions.

The temperature dependences of the magnetization of $Sm_{1-x}La_xFe_3(BO_3)_4$ single crystals with lanthanum concentrations $x = 0$, 0.5, and 0.75 are shown in Fig. 1. The magnetization was measured in a magnetic field of 0.1 T for magnetic field orientations along the crystallographic axis c (magnetization curves

$M_{\parallel}(T)$) and in the basal plane, or along the a axis (magnetization curves $M_{\perp}(T)$). In the paramagnetic region, the magnetization of all three samples is isotropic and obeys the Curie–Weiss law. The experimentally determined paramagnetic Curie temperatures were found to be equal to $\Theta_1 = -135$ K for $SmFe_3(BO_3)_4$, $\Theta_2 = -125$ K for $Sm_{0.5}La_{0.5}Fe_3(BO_3)_4$, and $\Theta_3 = -118$ K for $Sm_{0.25}La_{0.75}Fe_3(BO_3)_4$. The negative sign indicates the existence of the antiferromagnetic exchange interaction in the magnetic system. It can be seen that the absolute value of the paramagnetic Curie temperature decreases upon the substitution of nonmagnetic lanthanum ions La^{3+} for magnetic samarium ions Sm^{3+}. This suggests that there is an antiferromagnetic interaction of Sm^{3+} ions with the nearest neighbor iron ions Fe^{3+}.

At temperatures $T < T_N \sim 35$ K, the behavior of the magnetization for all compositions is not qualitatively different from the behavior observed earlier in $SmFe_3(BO_3)_4$ [5]. With a decrease in the temperature, the magnetization in the basal plane decreases monotonically, whereas along the c axis, it remains approximately equal to the value observed at the Néel temperature. This behavior indicates that the magnetic moments of iron ions Fe^{3+} are ordered in the basal plane. It can be seen from Fig. 1 that, with an increase in the concentration of La^{3+} ions, the magnetic moment per formula unit increases, and this increase is not related to the deviation of the magnetic moment from the plane, because the magnetization increases in both directions.

Figure 2 shows the experimental dependences of the magnetization on the magnetic field $M_{\parallel}(B)$ and $M_{\perp}(B)$ for $Sm_{1-x}La_xFe_3(BO_3)_4$ single crystals in the basal plane (Fig. 2a) and along the c axis (Fig. 2b) at the temperature $T = 2$ K. The magnetization curves measured for all compositions in magnetic fields $B >$ 2 T both in the basal plane and along the trigonal axis c differ only slightly from each other. This suggests that the processes of magnetization have the same character. The small difference in the magnetizations $M_{\parallel}(B)$ and $M_{\perp}(B)$ for the same value of the magnetic field (inset in Fig. 2b) is due to the influence of the magnetic uniaxial anisotropy. It can be seen from this figure that the initial part of the curve $M_{\perp}(B)$ for all compositions is nonlinear. Such behavior is observed for all easy-plane ferroborates. This is associated with the fact that, in trigonal crystals with the magnetic moments lying in the basal plane, there are three types of domains. In the case where the samples are magnetized in the basal plane in weak magnetic fields, the contribution to the magnetization comes from all three types of domains with the antiferromagnetic axes directed at an angle of 120° with respect to each other. In [9], the field dependence of the magnetization $M_{\perp}(B)$ was calculated in magnetic fields $B < 1.5$ T. In particular, it was shown that the processes of magnetization in different directions of the magnetic field in the basal plane occur in different ways. For the orientation of the magnetic field $\mathbf{B} \parallel \mathbf{a}$, it is a spin-flop transition in a domain with the antiferromagnetic axis along the a axis, whereas in the magnetic field $\mathbf{H} \parallel \mathbf{b}$, it is the depinning of 30-degree domain walls in a critical magnetic field.

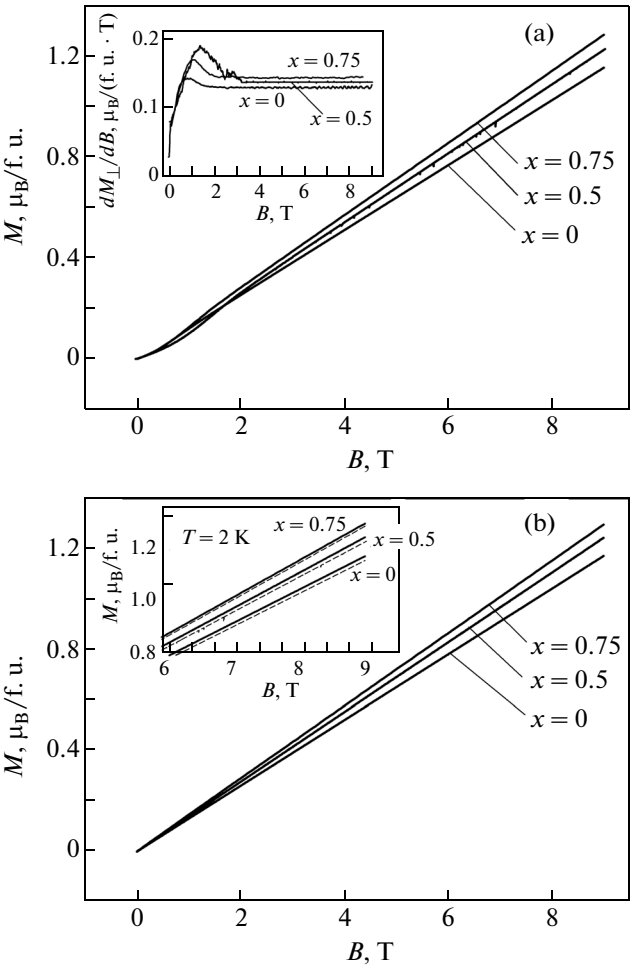

Fig. 2. Magnetization curves for $Sm_{1-x}La_xFe_3(BO_3)_4$ single crystals at $T = 2$ K for the magnetic field orientations (a) $\mathbf{B} \perp \mathbf{c}$ and (b) $\mathbf{B} \parallel \mathbf{c}$. The insets show (a) the derivative of the magnetization with respect to the field as a function of the magnetic field magnitude for the orientation $\mathbf{B} \perp \mathbf{c}$ and (b) magnetization curves for the orientations $\mathbf{B} \parallel \mathbf{c}$ (solid lines) and $\mathbf{B} \perp \mathbf{c}$ (dashed line) at $T = 2$ K.

It can be seen from Fig. 2a that the weak-field behavior of the magnetization is different for the compositions at different levels of doping with La^{3+} ions. This is best seen in the inset to Fig. 2a, which shows the magnetic susceptibility $dM_{\perp}/dB$. All the studied compositions are characterized by different rotations of domains in the direction of the magnetic field. The critical fields can be estimated from the position of the maximum in the curves. As can be seen from the inset to Fig. 2a, these fields for the compositions with differ-

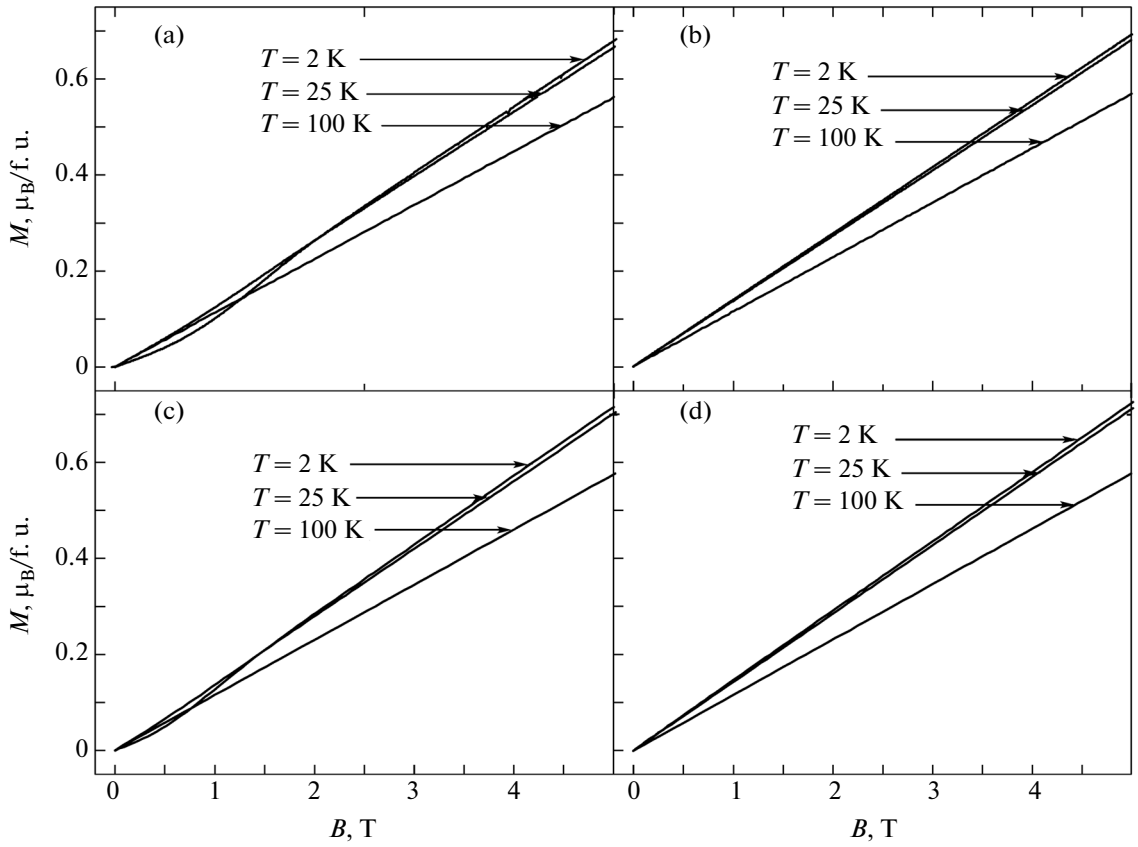

Fig. 3. Magnetization curves for (a, b) $Sm_{0.5}La_{0.5}Fe_3(BO_3)_4$ and (c, d) $Sm_{0.25}La_{0.75}Fe_3(BO_3)_4$ single crystals in magnetic fields (a, c) $\mathbf{B} \perp \mathbf{c}$ and (b, d) $\mathbf{B} \parallel \mathbf{c}$.

ent lanthanum concentrations are as follows: $B = 0.8$ T for the composition with $x = 0$, $B = 1.5$ T for $x = 0.5$, and $B = 1$ T for $x = 0.75$.

As the temperature increases, the behavior of the field dependences of the magnetization does not qualitatively change. The dependence $M_\parallel(B)$ is linear over the entire temperature range (Figs. 3b, 3d). The dependence $M_\perp(B)$ becomes linear below the transition temperature $T_N \approx 35$ K (Figs. 3a, 3c). Figure 3 shows the field dependences of the magnetizations $M_\perp(B)$ and $M_\parallel(B)$ for the compositions $Sm_{0.5}La_{0.5}Fe_3(BO_3)_4$ (Figs. 3a, 3b) and $Sm_{0.25}La_{0.75}Fe_3(BO_3)_4$ (Figs. 3c, 3d).

4. DISCUSSION OF THE RESULTS

The above results suggest a paradoxical situation: the substitution of nonmagnetic ions La^{3+} for magnetic ions Sm^{3+} in $Sm_{1-x}La_xFe_3(BO_3)_4$ ferroborates leads to an increase in the magnetic susceptibility. It seems a bit strange, because if we compare the magnetic susceptibilities of $SmFe_3(BO_3)_4$ and $YFe_3(BO_3)_4$ (the Y^{3+} ions, as well as the La^{3+} ions, are nonmagnetic), it turns out that the magnetic moment of the latter compound is less than that of the former compound in the entire measured temperature range and in magnetic fields up to 5 T. For example, for the orientation $\mathbf{B} \perp \mathbf{c}$ at $T = 2$ K in a magnetic field of 5 T, the $YFe_3(BO_3)_4$ compound has the magnetization $M_\perp = 0.58\ \mu_B$ per formula unit [13], whereas $SmFe_3(BO_3)_4$ at the same temperature and in the same magnetic field has the magnetization $M_\perp = 0.64\ \mu_B$ (Fig. 3). As the La^{3+} ions substitute for the Sm^{3+} ions, the magnetic moment becomes even higher. And if we could grow the stable trigonal phase $LaFe_3(BO_3)_4$, the magnetic moment of this compound would be obviously higher than the magnetic moment of $YFe_3(BO_3)_4$, even though the magnetic structure determined only by the iron sublattice is identical in both compounds. It is hard to say why this happens. We can only assume that the difference in the ionic radii of La^{3+} and Y^{3+} leads to a difference in the exchange interactions between the Fe^{3+} ions in the sequence Fe–O–Fe or Fe–O–B–O–Fe due to changes in the overlap integrals of the wave functions.

In our opinion, the above-described phenomenon should be explained by the competition of the *d–d* and *d–f* exchange interactions. The magnetic structure of rare-earth ferroborates with the huntite structure can be represented as follows [9] (Fig. 4): the magnetic

moments of iron ions are combined into two antiferromagnetically interacting sublattices, whereas samarium ions are not coupled by the exchange interaction with each other but antiferromagnetically interact with the nearest neighbor iron ions that are joined into one of the sublattices. In order to describe the observed magnetic properties of $Sm_{1-x}La_xFe_3(BO_3)_4$ crystals, we write the thermodynamic potential at $T = 0$ K by ignoring, for simplicity, the anisotropy in the basal plane:

$$F = F_{d-d} + F_{d-f} + F_{1d} + F_{1f} + F_Z, \quad (1)$$

where $F_{d-d} = \lambda_{d-d}\mathbf{M}_1\mathbf{M}_2$ is the exchange interaction energy of the iron sublattices; $F_{d-f} = \lambda_{d-f}(\mathbf{M}_1\mathbf{m}_1 + \mathbf{M}_2\mathbf{m}_2)$ is the exchange interaction energy of the iron sublattice with the samarium sublattice; $F_{1d} = K_{1d}[\cos^2(\theta_1^{Fe}) + \cos^2(\theta_2^{Fe})]$ and $F_{1f} = K_{1f}[\cos^2(\theta_1^{Sm}) + \cos^2(\theta_2^{Sm})]$ are the uniaxial magnetic anisotropy energies of the iron and samarium sublattices, respectively; and $F_Z = -\mathbf{H}(\mathbf{M}_1 + \mathbf{M}_2) - (\mathbf{m}_1 + \mathbf{m}_2)$ is the Zeeman interaction energy. Here, λ_{d-d} and λ_{d-f} are the exchange interaction constants and $K_{1d} > 0$ and $K_{1f} > 0$ are the uniaxial anisotropy constants. The magnetic moments of the ith iron sublattice $\mathbf{M}_i$ and the ith samarium sublattice $\mathbf{m}_i$ per formula unit are determined respectively by the formulas

$$\mathbf{M}_i = 3g_s\mu_B\langle\mathbf{S}_i\rangle, \quad \mathbf{m}_i = xg_J\mu_B\langle\mathbf{J}_i\rangle, \quad (2)$$

where $g_s = 2$ is the g-factor that takes into account only the spin moment of iron ions, $g_J = 2/7$ is the Landé factor for the samarium ion, $\mathbf{S}_i$ is the operator of the spin angular momentum of the iron ion, $\mathbf{J}_i$ is the operator of the total angular momentum of the samarium ion, and x is the concentration of samarium ions.

Let us consider the case where the external magnetic field $\mathbf{H}$ is directed along the c axis (Fig. 4a). Turning to writing the vectors $\mathbf{M}_i$ and $\mathbf{m}_i$ in the spherical coordinate system and taking into account that the vectors $\mathbf{H}$, $\mathbf{M}_i$, and $\mathbf{m}_i$ lie in one plane, we obtain

$$\begin{aligned} F &= \lambda_{d-d}M^2\cos(\theta_1^{Fe} - \theta_2^{Fe}) \\ &+ \lambda_{d-f}Mm[\cos(\theta_1^{Sm} - \theta_1^{Fe}) + \cos(\theta_2^{Sm} - \theta_2^{Fe})] \\ &+ K_{1d}(\cos^2\theta_1^{Fe} + \cos^2\theta_2^{Fe}) + K_{1f}(\cos^2\theta_1^{Sm} + \cos^2\theta_2^{Sm}) \\ &- HM(\cos\theta_1^{Fe} + \cos\theta_2^{Fe}) - Hm(\cos\theta_1^{Sm} + \cos\theta_2^{Sm})]. \end{aligned} \quad (3)$$

Here, M and m are the magnetic moments of the iron and samarium sublattices, respectively, and H is the external magnetic field.

In order to determine the equilibrium state of the magnetic structure, we minimize the thermodynamic potential with respect to the angles. Next, we introduce the following notation: $\theta_1^{Fe} = \frac{\pi}{2} - \theta^{Fe}$, $\theta_2^{Fe} = \frac{3\pi}{2} + \theta^{Fe}$, $\theta_1^{Sm} = \frac{3\pi}{2} + \theta^{Sm}$, and $\theta_2^{Sm} = \frac{\pi}{2} - \theta^{Sm}$ (Fig. 4a). As a result, we obtain the system of two independent equations

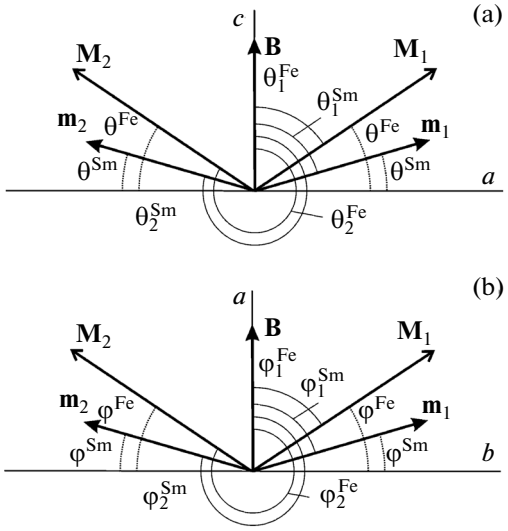

Fig. 4. Schematic representation of the magnetic structure of $Sm_{1-x}La_xFe_3(BO_3)_4$ single crystals in the magnetic field oriented along (a) the c axis and (b) the a axis.

$$\begin{aligned} &H_d\sin 2\theta^{Fe} + H_f\frac{m}{M}\sin(\theta^{Fe} + \theta^{Sm}) \\ &+ \frac{H_{1d}}{2}\sin 2\theta^{Fe} - H\cos\theta^{Fe} = 0, \end{aligned} \quad (4a)$$

$$H_f\sin(\theta^{Fe} + \theta^{Sm}) + \frac{H_{1f}}{2}\sin 2\theta^{Sm} - H\cos\theta^{Sm} = 0, \quad (4b)$$

where $H_d = \lambda_{d-d}M$, $H_f = \lambda_{d-f}M$, $H_{1d} = 2K_{1d}/M$, and $H_{1f} = 2K_{1f}/m$.

Unfortunately, the system of equations (4a) and (4b) does not have a solution in the analytical form. Therefore, we will restrict ourselves to the case where the angles θ^{Fe} and θ^{Sm} are small. This assumption is valid, because, for example, in $YFe_3(BO_3)_4$, where there is only the magnetic subsystem of iron, we have the angle $\theta^{Fe} \approx 2°$ in a magnetic field of 5 T at 2 K [13]. In this case, we can expand the angles θ^{Fe} and θ^{Sm} in a series by retaining only terms up to the first order of smallness. As a result, we obtain the following expressions for these angles taking into account that $H_{1d} \ll H_d$ and $H_{1f} \ll H_f$:

$$\theta^{Fe} = \left(1 - \frac{m}{M}\right)\frac{H}{2H_d + \frac{m}{M}H_{1f} + H_{1d}}, \quad (5a)$$

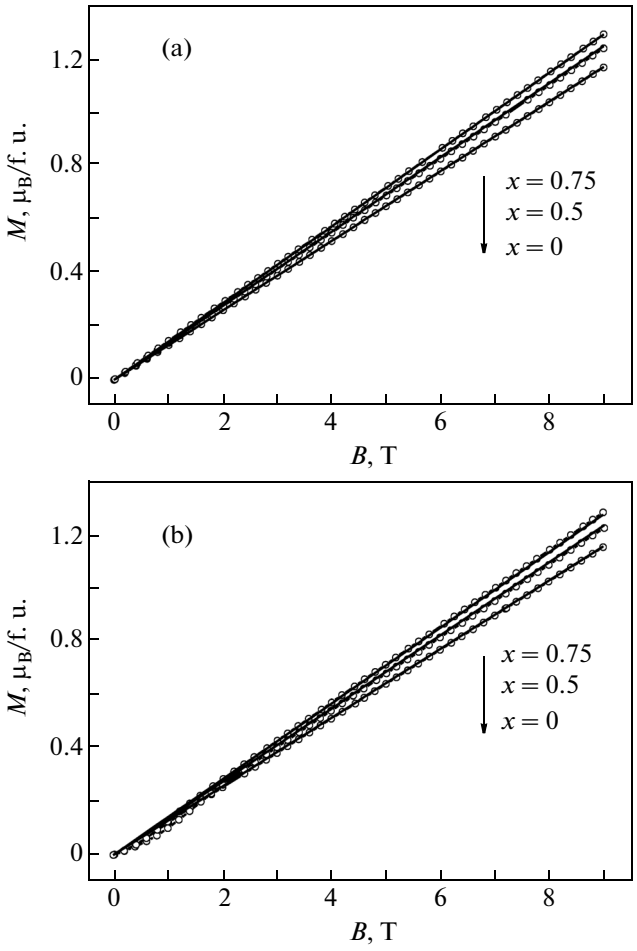

Fig. 5. Magnetization curves for $Sm_{1-x}La_xFe_3(BO_3)_4$ at $T = 2$ K: (a) $M_{||}(B)$ and (b) $M_{\perp}(B)$. Points are experimental data, and solid lines represent the results of the calculations.

$$\theta^{Sm} = \left[\frac{1}{H_f} - \left(1 - \frac{m}{M}\right)\frac{1}{2H_d + \frac{m}{M}H_{1f} + H_{1d}}\right]H. \quad (5b)$$

Similarly, by setting $H_{1d} = 0$ and $H_{1f} = 0$ in formula (3), we can obtain the following expressions for the angles in the case where the external magnetic field is directed in the basal plane without anisotropy in the basal plane:

$$\varphi^{Fe} = \left(1 - \frac{m}{M}\right)\frac{H}{2H_d}, \quad (6a)$$

$$\varphi^{Sm} = \left[\frac{1}{H_f} - \left(1 - \frac{m}{M}\right)\frac{1}{2H_d}\right]H, \quad (6b)$$

where φ^{Fe} and φ^{Sm} are the angles formed by the vectors $\mathbf{M}_i$ and $\mathbf{m}_i$ with the x axis, respectively (Fig. 4b).

The total magnetic moments for the magnetizations $M_{\perp}(B)$ and $M_{||}(B)$ per formula unit under the smallness condition for the angles are determined respectively by the formulas

$$M_{||} = M\theta^{Fe} + m\theta^{Sm}, \quad M_{\perp} = M\varphi^{Fe} + m\varphi^{Sm}. \quad (7)$$

Let the uniaxial anisotropy energy be denoted as $H_{eff} = \frac{m}{M}H_{1f} + H_{1d}$. Using neutron diffraction, the authors of [10] determined the magnetic moments of iron and samarium ions as follows: $\mu_{Fe} = 4.2\ \mu_B$ and $\mu_{Sm} = 0.24\ \mu_B$. By setting $M = 3\mu_{Fe}$ and $m = x\mu_{Sm}$ and varying the parameters H_d, H_f, and H_{eff}, we attempted to fit the dependences $M_{\perp}(B)$ and $M_{||}(B)$ to the experimental curves according to expressions (7), (6), and (5). However, any reasonable values of the parameters H_d, H_f, and H_{eff} could not satisfactorily describe the magnetization curves. Hence, in addition to these three parameters, we also varied the magnetic moment of the samarium ion μ_{Sm}.

Figure 5 presents the results of the calculation of the dependences $M_{\perp}(B)$ and $M_{||}(B)$ in comparison with the experimental data. The best agreement is achieved at the following values of the fitting parameters: $H_d = 43$ T, $H_f = 90$ T, $H_{eff} = -1.2$ T, and $m = 1.7\ \mu_B$. The obtained parameters are somewhat different from the previously calculated values. For example, in [4], $H_d = 64$ T and $H_f = 30$ T, whereas in [9], $H_d = 59$ T and $H_f = 53$ T. It should be noted that, in [7], the magnetic field of the f–d exchange interaction $H_f = 94$ T was determined from the splitting of the ground doublet of the samarium ion Sm^{3+}, which agrees most closely with our results.

The negative value of H_{eff} indicates that the magnetization $M_{||}(B)$ has higher values than $M_{\perp}(B)$ for the same temperatures and magnetic fields (inset in Fig. 2b). The result is unexpected, because the temperature dependences of the magnetization (Fig. 1) and neutron diffraction data [10] suggests that the $Sm_{1-x}La_xFe_3(BO_3)_4$ ferroborate is characterized by the easy-plane anisotropy. This result is difficult to explain. We can only assume that the observed decrease in the magnetization, when the magnetic field is applied in the basal plane, is caused by the presence of magnetic domains with the antiferromagnetic axes directed at an angle of 120° with respect to each other.

5. CONCLUSIONS

Single crystals of rare-earth ferroborates $Sm_{1-x}La_xFe_3(BO_3)_4$ ($x = 0$, 0.5, 0.75) were grown by the flux method using bismuth trimolybdate. The grown single crystals were investigated using the X-ray diffraction analysis. The phase purification of the samples was performed and the lattice parameters were determined. The magnetic properties of the single

crystals were investigated in wide ranges of temperatures and magnetic fields.

It was found that the substitution of nonmagnetic ions La^{3+} for magnetic ions Sm^{3+} in $Sm_{1-x}La_xFe_3(BO_3)_4$ ferroborates leads to an increase in the magnetic moment of the compound. The behavior of the magnetic properties of the grown single crystals was explained qualitatively in the framework of the phenomenological model. The parameters of *d–d* and *d–f* exchange interactions were estimated. The previously found field of the *f–d* exchange interaction $H_f = 94$ T [7], which was determined from the splitting of the ground doublet of the samarium ion Sm^{3+}, agrees very well with our result $H_f = 90$ T. This is not true for the field of the *d–d* exchange interaction, which was found to be approximately 1.5 times less than the values estimated in earlier studies [4, 9].

We note that there is a need for further investigation of the magnetic structure of $Sm_{1-x}La_xFe_3(BO_3)_4$ crystals. For a full understanding of the whole picture, it is necessary to perform neutron diffraction investigations in magnetic fields.

ACKNOWLEDGMENTS

This study was supported by the Russian Foundation for Basic Research (project no. 14-02-00307_a) and the Ministry of Education and Science of the Russian Federation within the framework of the State Task for the Russian Siberian Federal University for Implementation of Scientific Research Work in 2014 (assignment no. 3.2534.2014/K).

REFERENCES

1. A. K. Zvezdin, S. S. Krotov, A. M. Kadomtseva, G. P. Vorob'ev, Yu. F. Popov, A. P. Pyatakov, L. N. Bezmaternykh, and E. N. Popova, JETP Lett. **81** (6), 272 (2005).
2. A. K. Zvezdin, G. P. Vorob'ev, A. M. Kadomtseva, Yu. F. Popov, A. P. Pyatakov, L. N. Bezmaternykh, A. V. Kuvardin, and E. A. Popova, JETP Lett. **83** (11), 509 (2006).
3. A. N. Vasiliev and E. A. Popova, Low Temp. Phys. **32** (8), 735 (2006).
4. A. M. Kadomtseva, Yu. F. Popov, G. P. Vorob'ev, A. P. Pyatakov, S. S. Krotov, K. I. Kamilov, V. Yu. Ivanov, A. A. Mukhin, A. K. Zvezdin, A. M. Kuz'menko, L. N. Bezmaternykh, I. A. Gudim, and V. L. Temerov, Low Temp. Phys. **36** (6), 511 (2010).
5. Yu. F. Popov, A. P. Pyatakov, A. M. Kadomtseva, G. P. Vorob'ev, A. K. Zvezdin, A. A. Mukhin, and V. Yu. Ivanov, J. Exp. Theor. Phys. **111** (2), 199 (2010).
6. A. A. Mukhin, G. P. Vorob'ev, V. Yu. Ivanov, A. M. Kadomtseva, A. S. Narizhnaya, A. M. Kuz'menko, Yu. F. Popov, L. N. Bezmaternykh, and I. A. Gudim, JETP Lett. **93** (5), 275 (2011).
7. E. P. Chukalina, M. N. Popova, L. N. Bezmaternykh, and I. A. Gudim, Phys. Lett. A **374**, 1790 (2010).
8. A. M. Kuz'menko, A. A. Mukhin, V. Yu. Ivanov, A. M. Kadomtseva, and L. N. Bezmaternykh, JETP Lett. **94** (4), 294 (2011).
9. A. A. Demidov, D. V. Volkov, I. A. Gudim, E. V. Eremin, and V. L. Temerov, J. Exp. Theor. Phys. **116** (5), 800 (2013).
10. C. Ritter, A. Pankrats, I. Gudim, and A. Vorotynov, J. Phys.: Condens. Matter. **24**, 386002 (2012).
11. L. N. Bezmaternykh, V. L. Temerov, I. A. Gudim, and N. A. Stolbovaya, Crystallogr. Rep. **50**, 97 (2005).
12. Y. Hinatsu, Y. Doi, K. Ito, M. Wakeshima, and A. Alemi, J. Solid State Chem. **172**, 438 (2003).
13. E. A. Popova, A. N. Vasiliev, V. L. Temerov, L. N. Bezmaternykh, N. Tristan, R. Klingeler, and B. Büchner, J. Phys.: Condens. Matter **22**, 116006 (2010).

Translated by O. Borovik-Romanova